

## Recruitment of endocytosis in sonopermeabilization-mediated drug delivery: a real-time study

This content has been downloaded from IOPscience. Please scroll down to see the full text.

2015 Phys. Biol. 12 046010

(<http://iopscience.iop.org/1478-3975/12/4/046010>)

View [the table of contents for this issue](#), or go to the [journal homepage](#) for more

Download details:

IP Address: 143.121.237.84

This content was downloaded on 23/02/2016 at 13:07

Please note that [terms and conditions apply](#).

## Physical Biology



## PAPER

## Recruitment of endocytosis in sonopermeabilization-mediated drug delivery: a real-time study

## OPEN ACCESS

## RECEIVED

15 January 2015

## REVISED

27 May 2015

## ACCEPTED FOR PUBLICATION

3 June 2015

## PUBLISHED

29 June 2015

Content from this work may be used under the terms of the [Creative Commons Attribution 3.0 licence](#).

Any further distribution of this work must maintain attribution to the author(s) and the title of the work, journal citation and DOI.



Marc Derieppe<sup>1,4</sup>, Katarzyna Rojek<sup>1,2,4</sup>, Jean-Michel Escoffre<sup>1</sup>, Baudouin Denis de Senneville<sup>1,3</sup>, Chrit Moonen<sup>1</sup> and Clemens Bos<sup>1</sup>

<sup>1</sup> Imaging Division, University Medical Center Utrecht, Utrecht, Netherlands

<sup>2</sup> Laboratory of Synaptogenesis, Cell Biology Department, Nencki Institute of Experimental Biology, Polish Academy of Sciences, Warsaw, Poland

<sup>3</sup> Institut de Mathématiques de Bordeaux, UMR 5251, CNRS, Université Bordeaux, Bordeaux, France

<sup>4</sup> The authors contributed equally to this work.

E-mail: [m.derieppe@umcutrecht.nl](mailto:m.derieppe@umcutrecht.nl)

**Keywords:** sonoporation, endocytosis, drug delivery, pharmacokinetic parameters, real time, fibered confocal fluorescence microscopy

Supplementary material for this article is available [online](#)

### Abstract

Microbubbles (MBs) in combination with ultrasound (US) can enhance cell membrane permeability, and have the potential to facilitate the cellular uptake of hydrophilic molecules. However, the exact mechanism behind US- and MB-mediated intracellular delivery still remains to be fully understood. Among the proposed mechanisms are formation of transient pores and endocytosis stimulation. In our study, we investigated whether endocytosis is involved in US- and MB-mediated delivery of small molecules. Dynamic fluorescence microscopy was used to investigate the effects of endocytosis inhibitors on the pharmacokinetic parameters of US- and MB-mediated uptake of SYTOX Green, a 600 Da hydrophilic model drug. C6 rat glioma cells, together with SonoVue<sup>®</sup> MBs, were exposed to 1.4 MHz US waves at 0.2 MPa peak-negative pressure. Collection of the signal intensity in each individual nucleus was monitored during and after US exposure by a fibered confocal fluorescence microscope designed for real-time imaging. Exposed to US waves, C6 cells pretreated with chlorpromazine, an inhibitor of clathrin-mediated endocytosis, showed up to a 2.5-fold significant increase of the uptake time constant, and a 1.1-fold increase with genistein, an inhibitor of caveolae-mediated endocytosis. Both inhibitors slowed down the US-mediated uptake of SYTOX Green. With C6 cells and our experimental settings, these quantitative data indicate that endocytosis plays a role in sonopermeabilization-mediated delivery of small molecules with a more predominant contribution of clathrin-mediated endocytosis.

### Introduction

In oncology, microbubble (MB)-assisted ultrasound (US) was introduced as a promising method to improve therapeutic efficacy of drugs by increasing their local delivery. In the presence of MBs, tissue exposure to US waves transiently increases the permeability of biological barriers, such as cell membranes and blood vessels, to increase the intracellular uptake of drugs or enhance drug extravasation, respectively [1–3]. Specifically, MB-assisted US is used to circumvent poor transendothelial transport, and transmembrane transport of hydrophilic anticancer drugs, such as DNA intercalating agents, i.e. gemcitabine [4] or

irinotecan [5]. The potential of this approach for cancer therapy is clearly shown in an increasing number of publications on preclinical [6–9] and clinical [4] drug delivery using MB-assisted US.

Many studies have found that US-mediated plasma membrane permeabilization results from the formation of transient pore-like structures in the plasma membrane, thus facilitating the delivery of molecules of different molecular weights into the intracellular compartment [10–12]. Hence, this phenomenon was named sonoporation [13]. The cause of these transient structures in the plasma membrane is commonly assumed to be acoustic cavitation [10]. The use of US contrast agents (i.e. gaseous MBs) may

enhance this effect by initiating the nucleation of the cavitation [14] in this vicinity, and reduces the required energy deposition in the tissues during US exposure. Cavitation can be categorized either as (1) inertial cavitation, which involves rapid growth and collapse of MBs [14], or as (2) stable cavitation with an oscillatory motion of bubbles with fluid microstreamings exerting shear forces on the plasma membrane [14]. Both induce transient and local cell membrane permeabilization. At the single-cell level, MBs were reported to permeabilize a neighboring cell when the distance between the MB shell and the plasma membrane equaled at most three times the MB diameter [15]. Therefore, sonopermeabilization protocols consist of mixing MBs with cells *in vitro*, or *in vivo* injecting them intravascularly or intratumorally to ensure the close vicinity of MBs with endothelial and tumor cells. Recently, in a clinical case study using combined US and SonoVue® MBs to enhance gemcitabine delivery in a patient suffering from pancreatic cancer [4], 0.5 mL of clinically approved MBs followed by 5 mL of saline were injected intravenously every 3.5 min throughout the 1 h treatment.

However, there is increasing evidence that cavitation-mediated mechanical stimuli, as well as static tensile forces [16], induce the recruitment of endocytosis in US and MB-mediated drug [17, 18] and gene delivery [19, 20]. Using endocytosis inhibitors, such as chlorpromazine [18] and genistein [21], previous studies [22] showed that clathrin- and caveolae-mediated pathways were recruited for the US-mediated intracellular delivery of macromolecules, such as dextran from 4.4 to 500 kDa. Other studies suggested a selective contribution of one of the two endocytosis pathways: clathrin-mediated endocytosis has been proposed to facilitate the internalization of plasmid DNA [22] whereas caveolae-mediated endocytosis has been suggested to promote the delivery of fluorescently tagged proteins into endothelial cells [23]. However, to our knowledge, few studies providing real-time quantitative information of model drug uptake upon US exposure have been conducted so far at the single-cell level [24] and in a cell population [25].

Previously, we showed that the real-time monitoring of the uptake of SYTOX Green model drug upon US exposure was feasible using a dedicated setup incorporating a fibered confocal fluorescence microscope (FCFM) [26]. From the image sequence displaying the fluorescence signal enhancement of a cell population of more than a hundred of cells, the pharmacokinetic parameters of each cell were accurately assessed by implementing a complete post-processing pipeline, which was automated from the data pre-processing to the statistical analysis of the population kinetic data [26]. We used SYTOX Green intercalating dye, which is cell impermeable and exhibits fluorescence intensity upon binding to nucleic acids, making it a probe of plasma membrane permeabilization [27].

Here, we test the hypothesis that endocytosis is recruited for US-mediated intracellular delivery of 600 Da SYTOX Green model drug. Specifically, we investigate the effect of endocytosis inhibitors on the pharmacokinetic parameters derived from the real-time monitoring of SYTOX Green uptake.

## Materials and methods

### Cell culture

C6 rat glioma cells (ATCC® number: CCL-107™) were grown as a monolayer in Dulbecco's modified Eagle's medium (DMEM, Sigma-Aldrich®, St. Louis, MO) with low glucose concentration ( $1 \text{ g L}^{-1}$ ) and stable glutamine supplemented with 10% fetal bovine serum (Sigma-Aldrich®) and 1% penicillin–streptomycin (Sigma-Aldrich®). The cells were routinely subcultured every 4 days and incubated at 37 °C in humidified atmosphere with a 5% CO<sub>2</sub> incubator. This cancer cell line is frequently used to develop and optimize sonopermeabilization for drug and gene delivery [28–30].

### Endocytosis inhibitors

Cells were incubated in the presence of two endocytosis inhibitors: (1) chlorpromazine (Sigma-Aldrich®), an inhibitor of clathrin-mediated endocytosis, from 10 to 60  $\mu\text{M}$ . Chlorpromazine translocates clathrin together with its adapter protein from the plasma membrane to intracellular vesicles, thus hindering the formation of clathrin-coated pits at the cell surface [31]; (2) Genistein (Sigma-Aldrich®), an inhibitor of caveolae-mediated endocytosis from 200  $\mu\text{M}$ , typical minimum concentration for efficient and non-toxic effect of genistein for C6 cells [32], to 300  $\mu\text{M}$ . Genistein hinders caveolae-coated vesicle internalization by blocking dynamin-2 ring assembly, which is critical for late stages of membrane invagination [33].

### Selection of the inhibitor concentration—cell viability assessment

XTT assays, which are based on metabolic turnover of tetrazolium dye by living cells, were performed to determine a concentration range of chlorpromazine and genistein to study their effect while limiting their cytotoxicity. Neither US waves nor MBs have been used in these assays.  $5 \times 10^3$  cells/well were seeded in a 96-well plate for 20 h and subsequently incubated at 37 °C and 5% CO<sub>2</sub> with complete DMEM medium containing either 50–300  $\mu\text{M}$  genistein, or 10–100  $\mu\text{M}$  chlorpromazine for 30 min. After incubation, 50  $\mu\text{L}$  XTT solution (XTT Cell Proliferation Assay Kit—ATCC®, Netherlands) was added to each well, which was prepared by adding 100  $\mu\text{L}$  solution of 1-methoxy phenazine methosulfate to 5 mL of XTT. Cells were then further incubated at 37 °C, 5% CO<sub>2</sub> for 1 h. The absorbance of colored formazans was measured at

492 nm using an EZ Read 400 Microplate reader (Biochrom, Cambridge, United Kingdom), and corrected for the reference absorbance at 620 nm. Measured absorbance values were normalized by the absorbance without inhibitor. All tests were performed at least in quadruplicate. Subsequently, the influence of the incubation time in the presence of the inhibitor was evaluated by assessing the cytotoxicity at 0.5, 1.5 and 3 h of incubation with the selected inhibitor concentrations. These incubation times were chosen based on the expected duration of the FCFM experiment. Results were presented as mean  $\pm$  standard error of the mean (SEM).

### Sensitivity and specificity of the inhibitors

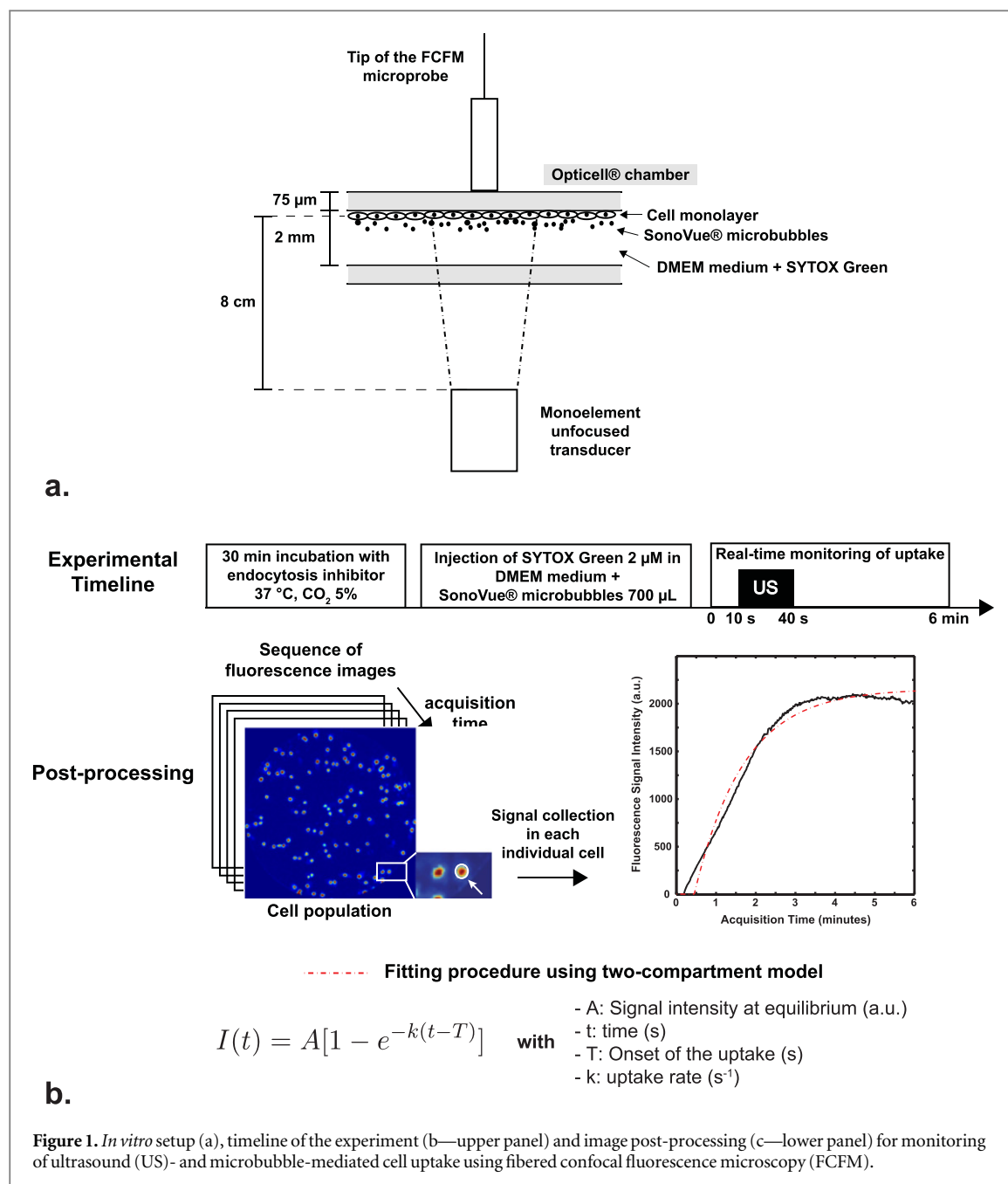
Sensitivity and specificity of chlorpromazine and genistein endocytosis inhibitors were evaluated by staining clathrin and caveolae vesicles with  $50 \mu\text{g mL}^{-1}$  Human transferrin (HTr)—Alexa Fluor 488 nm conjugate (Sigma-Aldrich<sup>®</sup>) and  $10 \mu\text{g mL}^{-1}$  Cholera Toxin (Chol Tox)—Alexa Fluor 488 nm conjugate (Sigma-Aldrich<sup>®</sup>), respectively. Here, neither US waves nor MBs have been used in this evaluation. First, C6 cells were seeded in  $\mu$ -slide 4 well glass bottom chamber (ibidi GmbH, Germany) for three days and reached 90% confluency at the day of the experiment ( $7 \times 10^4$  cells/well). The cells were once washed with Phosphate Buffer Saline (PBS) and their medium was changed to cell culture medium without serum. After inhibitor addition, the cells were further incubated for 30 min at 37 °C and 5% CO<sub>2</sub>. Subsequently, HTr or Chol Tox was added and the cells were incubated with the inhibitor and the marker for 1 h. For cell viability assessment, propidium iodide (PI) at  $0.1 \mu\text{g mL}^{-1}$  was added to the cells, followed by incubation for 10 min. The medium was then removed, and the cells were thrice washed with PBS with Ca<sup>2+</sup> and Mg<sup>2+</sup>. Finally, cells were fixed for 20 min using 4% paraformaldehyde in PBS, and stored in PBS with Ca<sup>2+</sup> and Mg<sup>2+</sup>. Fluorescence images of the endocytosis vesicles were collected with a laser scanning confocal fluorescence microscope (LSM 700, AxioObserver, Carl Zeiss Microscopy GmbH, Jena, Germany) and a Plan-Apochromat 63x oil-immersion objective, 1.4 numerical aperture, 488 and 555 nm excitation wavelengths, a  $0.1 \mu\text{m}$  numerical spatial resolution, and a  $1024 \times 1024$ -pixel matrix.

### Assessment of the uptake kinetics in the presence of the endocytosis inhibitors—real-time imaging

Real-time monitoring of the US-mediated model drug uptake was based on the use of SYTOX Green intercalating fluorescent dye (Life Technologies<sup>™</sup>, Saint-Aubin, France) (Excitation 504 nm/Emission 523 nm) [25]. This small molecular-weight (600 Da) fluorescent dye is cell-impermeable, and exhibits a 100-to 1000-fold increase in fluorescence upon

binding to nucleic acids [34], thus making it a probe for US-mediated cell plasma membrane uptake [35].

As previously described, OptiCell<sup>™</sup> culture chambers (Thermo Fischer Scientific, Rochester, NY, USA) were seeded with  $4 \times 10^6$  cells 48 h prior to the experiment. C6 cells grow as an adherent monolayer in this culture chamber, favoring the contact between the MBs and the plasma membranes of the cells. Using SYTOX Green as a model drug and this culture chamber, paracellular transports are outside the scope of this study. On the day of the experiment, cells displayed 80–90% confluence and were provided with fresh complete DMEM medium. Then, cells were exposed to the inhibitor for 30 min at 37 °C, 5% CO<sub>2</sub>, but also during the subsequent imaging session lasting between 1 h and 2.5 h. In the presence of the endocytosis inhibitors, the impact of this incubation time on the uptake kinetics was evaluated, and showed no significant difference (Kruskall–Wallis (KW) test,  $p > 0.05$ ) (data not shown). Subsequently, SYTOX Green at a final concentration of  $2 \mu\text{M}$  and a commercially available US contrast agent (SonoVue<sup>®</sup>, Bracco, Milan, Italy) at a ratio of 20 MBs per cell were added to the cell culture chamber. The OptiCell<sup>™</sup> wall containing the cell monolayer was placed upwards to favor contacts between the cell monolayer and the MBs subjected to the buoyancy. The US setup consisted of a 20 mm diameter unfocused mono-element US transducer (Precision Acoustics, model TPZT, serial number PA 449, Dorchester, UK) positioned 8 cm below the OptiCell<sup>™</sup> cell-culture chamber (figure 1(a)). Cells were exposed to US waves for 30 s, with the following settings: 1.4 MHz central frequency, 10% duty cycle with 1 kHz pulse repetition frequency to trigger MB cavitation, 0.2 MPa peak negative acoustic pressure yielding a low mechanical index of 0.2 suitable for drug delivery. As reported previously [36], the two OptiCell<sup>™</sup> membranes attenuated less than 2% of the energy of the US beam. Using a  $100 \mu\text{s}$  pulse, the water surface was 10 cm above the OptiCell<sup>™</sup>, which prevented the buildup of standing waves. Generating only stable cavitation, these acoustic parameters have been optimized to induce an efficient and transient membrane permeabilization while limiting cell detachment and cell mortality (unpublished data). The choice of the central frequency was guided by the highest acoustic yield of the transducer, i.e. 1.4 MHz, which implies a slight compromise with respect to the center of the absorption peak of the SonoVue<sup>®</sup> MBs at the sub-harmonic frequency, i.e. 1.7 MHz [37]. Fibered Confocal Fluorescence Microscopy (CellVizio<sup>®</sup>, Mauna Kea Technologies, Paris, France) was conducted with an excitation wavelength of 488 nm. Imaging sequences were collected during 6 min at 8.5 frames per second, with the 30 s sonication starting after 10 s of imaging (figure 1(b)). The fluorescence images were acquired at a working distance of  $100 \mu\text{m}$ , a lateral resolution of  $3.9 \mu\text{m}$  and a field of view of  $593 \times 593 \mu\text{m}$ . For each inhibitor concentration, the experiment was



performed at least in triplicate. Each imaging session started with a control experiment, in which cells were not subjected to any endocytosis inhibitor.

#### Data analysis

Uptake kinetics of SYTOX Green were obtained from the real-time fluorescence data as described in [26]. The cell nuclei were detected using the Radial-Symmetry-Transform algorithm [38], and tracked frame-by-frame using an Iterative-Closest-Point algorithm [26]. The fluorescence signal intensity profiles were then analyzed for each nucleus individually (figure 1(b)). A two-compartment model was proposed to represent the extracellular space and the intracellular compartment, separated by a plasma membrane. This model neglected the diffusion of

SYTOX Green in the cytoplasm and the crossing of the nuclear membrane, as previous studies indicated that these two steps were extremely rapid for molecules with a molecular weight lower than 5 kDa [39, 40]. The corresponding signal intensity ( $I$ ) is as follows:

$$I(t) = A[1 - \exp(-k(t - T))],$$

where  $A$  is the asymptotic signal enhancement,  $T$  the time of signal onset, and  $k$  the uptake rate. The model was considered accurate when Pearson's correlation coefficient ( $r^2$ ) was greater than 0.95; the values of the uptake rate of SYTOX Green were reported as median with interquartile ranges.

The statistical analysis was performed using GraphPad Prism software (La Jolla, CA, USA). To evaluate the viability of C6 cells preincubated during 30 min, each cell population exposed to a

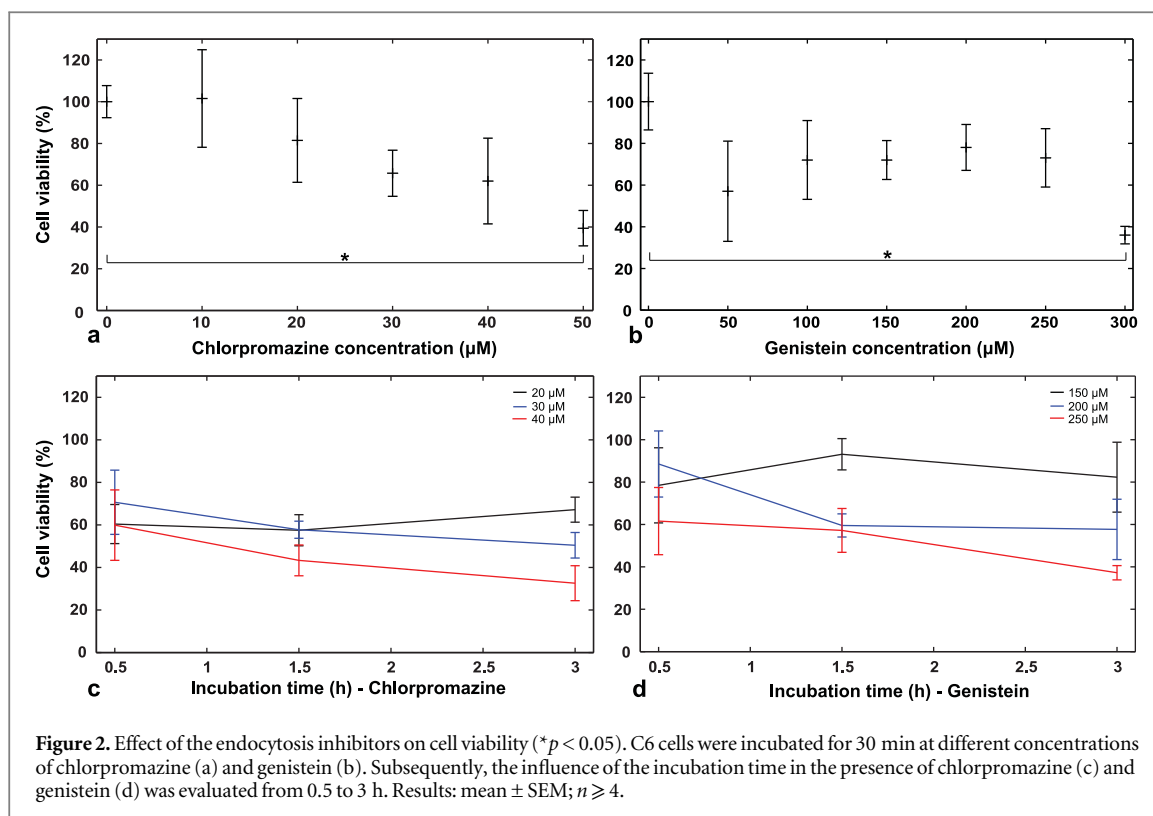


**Figure 2.** Effect of the endocytosis inhibitors on cell viability ( $*p < 0.05$ ). C6 cells were incubated for 30 min at different concentrations of chlorpromazine (a) and genistein (b). Subsequently, the influence of the incubation time in the presence of chlorpromazine (c) and genistein (d) was evaluated from 0.5 to 3 h. Results: mean  $\pm$  SEM;  $n \geq 4$ .

concentration of endocytosis inhibitor was compared to the one without endocytosis inhibitor, i.e. the reference population, using the unpaired non-parametric Mann–Whitney test (MW), as the values of viability in the cell populations were not distributed normally. The effect of the incubation time on cell viability was tested using the unpaired non-parametric KW test. The distributions of time constants obtained from two inhibitor concentrations were compared using the MW test. For all the tests, the results were considered significant when  $p$  was lower than 0.05.

Results derived from control experiments were collected until the end of the study and two separate control data sets were created. In the first set, we accumulated all control data for genistein, i.e., all control data from the same days when the different concentrations of genistein (200, 250 and 300  $\mu\text{M}$ ) were tested. The second consisted of all control data for chlorpromazine. For each inhibitor concentration, FCFM experiments were performed at least three times.

## Results

### Selection of the inhibitor concentration—cell viability assessment

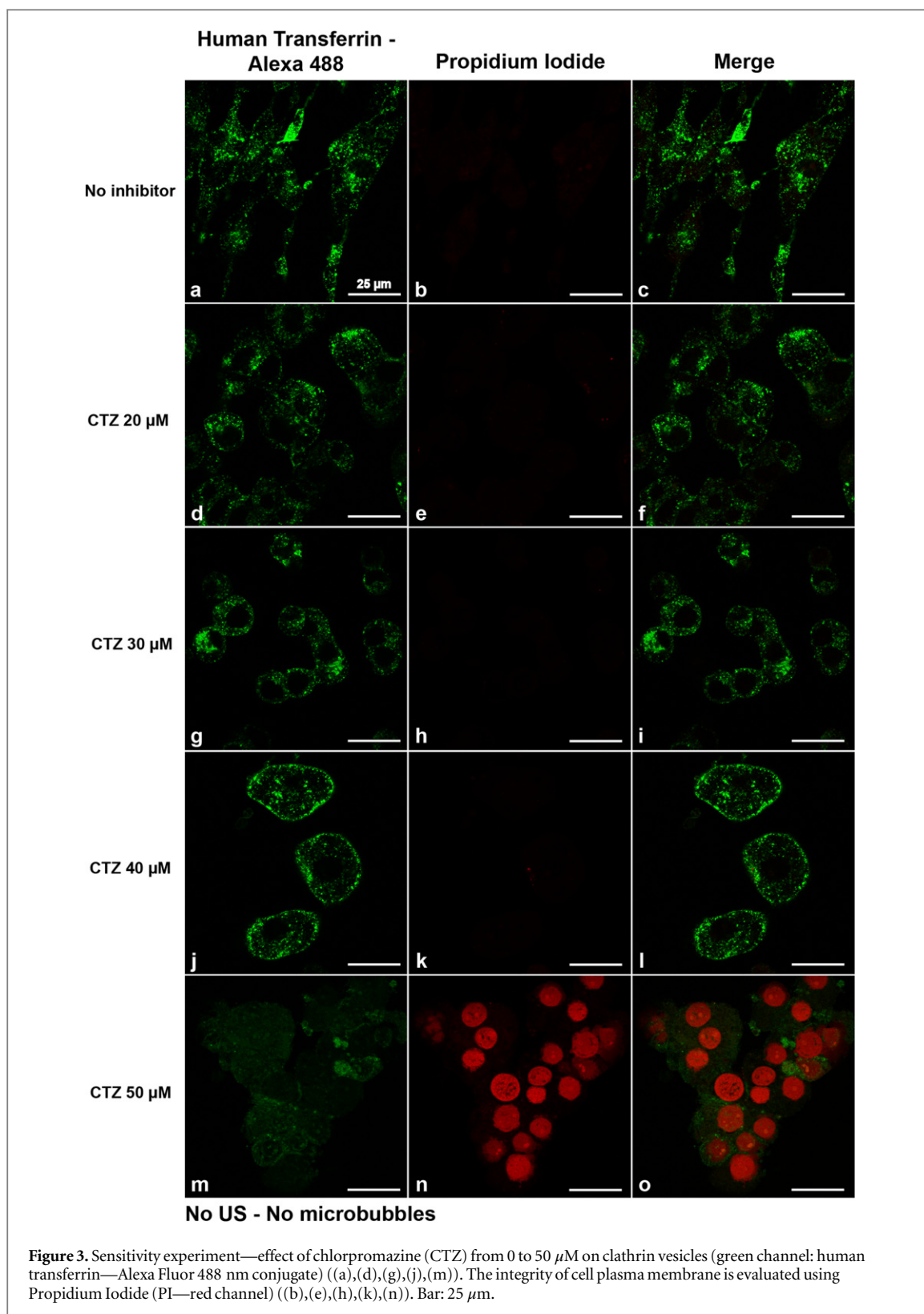
At high concentrations, both endocytosis inhibitors have an effect on the viability of C6 cells, which were for these experiments not exposed to US and MBs. According to the XTT absorbance data, a loss of cell viability was noticed from 20  $\mu\text{M}$  of chlorpromazine, followed by a continuous decrease, until reaching a significant loss below 50% at 50  $\mu\text{M}$  (MW,  $p < 0.05$ )

(figure 2(a)). Conversely, cell viability was not affected by genistein in a dose-dependent manner: a plateau of 70% viability was observed until a significant decrease of viability at 300  $\mu\text{M}$  of genistein (MW,  $p < 0.05$ ) (figure 2(b)).

The influence of the incubation time on cell viability was evaluated at 0.5, 1.5 and 3 h of incubations with concentrations of chlorpromazine (figure 2(c)) and genistein (figure 2(d)) for which cell viability was over 50%. The cytotoxic effect of 20  $\mu\text{M}$  chlorpromazine is relatively stable and was approximately 60% from 0.5 to 3 h of incubation time. For higher chlorpromazine concentrations, the cell viability decreased by 10–20% when the incubation time extended to 1.5 and 3 h. No significant difference was found in each of the three concentrations (KW,  $p > 0.05$ ). Concerning genistein, an effect of the incubation time on cell viability was observed for concentrations above 200  $\mu\text{M}$ , with a non-significant decrease of cell viability of up to a 20–30% with an incubation time of 3 h (KW,  $p > 0.05$ ). These data suggest that the cytotoxicity variations are acceptable in the presence of chlorpromazine or genistein during the time needed to perform the FCFM session.

### Inhibition specificity and cell sensitivity

The sensitivity of C6 cells to the inhibitors, in the absence of US and MBs, was determined by staining clathrin and caveolae vesicles, and observing cell morphology by laser scanning confocal microscopy. Without inhibitor, cells showed an elongated cytoplasm (figure 3(a)), which is typical of glial cells,



indicating integrity of the cytoskeleton. The absence of PI signal in the nucleus indicated that cell plasma membranes are intact (figure 3(b)). Stained with HTr with Alexa Fluor 488 conjugate, punctiform clathrin vesicles were distributed in the cytoplasm. As CTZ concentration increased, C6 glioma cells first lost their elongated shape, which would suggest that

cytoskeleton activity is hampered at this concentration (figures 3(d) and (g)). However, the distribution of stained clathrin vesicles remained apparently homogeneous in the cytoplasm. At 40  $\mu\text{M}$  (figure 3(j)), the absence of elongated cytoskeleton was also observable, and clathrin vesicles are predominantly located at the plasma membranes, according to the high

fluorescence signal densely expressed at this site, also observed in Vercauteren *et al* [33]. This suggests that chlorpromazine indeed impedes clathrin-mediated transport. At 50  $\mu\text{M}$  of chlorpromazine (figure 3(m)), only a diffuse background fluorescence was noticed in cell cytoplasm with few vesicles. At this concentration, PI fluorescence signal is present at the nucleus, indicating that chlorpromazine affected the integrity of the plasma membranes (figure 3(n)).

Moreover, the specificity of chlorpromazine specificity was verified by exposing cells whose caveolae vesicles were stained with Cholera Toxin—Alexa Fluor 488 conjugate to the clathrin-vesicle inhibitor (figures S1(d), (g), (j), and (m)). From 20 to 40  $\mu\text{M}$  of chlorpromazine, caveolae vesicles stained with Cholera toxin were distributed homogeneously in the cytoplasm, suggesting that chlorpromazine did not impede trafficking of caveolae vesicles (figures S1(d), (g), and (j)). Again, cells exposed to chlorpromazine at 50  $\mu\text{M}$  showed a diffuse background signal with PI signal present in the nuclei, suggesting that the integrity of plasma membrane was affected (figure S1(n)).

In the presence of genistein from 200 to 300  $\mu\text{M}$ , staining of caveolae vesicles with Cholera Toxin—Alexa Fluor 488 conjugate showed an acute inhibition of caveolae-mediated pathway in the cytoplasm (figures 4(d), (g), and (j)), according to the low number of caveolae vesicles in the cytoplasm compared to the control without inhibitor. No PI fluorescence signal is present in cell nuclei, suggesting good cell integrity (figures 4(b), (e), (h), and (k)).

Conversely, staining of clathrin vesicles showed images in the presence of genistein from 200 to 300  $\mu\text{M}$  comparable to the images without inhibitor (figures S2(d), (g), and (j)), with punctiform structures homogeneously distributed in the cytoplasm. Here, the elongated shape of the plasma membranes confirms the integrity of the cytoskeleton, also suggested by the absence of PI fluorescence signal in the nuclei. Thus, genistein did not inhibit clathrin-mediated pathway in the range of concentrations investigated here. In the scope of our study, genistein and chlorpromazine can therefore be considered specific and effective inhibitors of endocytosis in C6 cells.

#### Assessment of the uptake kinetics in the presence of the endocytosis inhibitors—real-time imaging

In a sonopermeabilization experiment, C6 cells exposed to genistein showed a statistically significant but modest (MW,  $p < 0.05$ ) increase of the uptake time constant  $1/k$  of SYTOX Green, from 52 s (20 s,  $n = 451$ ) without inhibitor to 58 s (22 s,  $n = 352$ ) at 300  $\mu\text{M}$  of genistein, respectively (figures 5 and S3(a) and (c)). Also, time-constant differences between 200 and 250  $\mu\text{M}$ , and between 200  $\mu\text{M}$  and 300  $\mu\text{M}$  of genistein were statistically significant (MW,  $p < 0.05$ ). These data suggest that caveolae-mediated pathway has a low recruitment level during

sonopermeabilization-stimulated uptake for this cell line and our US settings.

Cells in the presence of chlorpromazine showed a dose-dependent slowing down of SYTOX Green uptake from 52 s (22 s,  $n = 946$ ) without treatment to 2 min 11 s (1 min 33 s,  $n = 262$ ) at 40  $\mu\text{M}$  of chlorpromazine, respectively (figures 6 and S3(b) and (c)). All distributions from 0 to 50  $\mu\text{M}$  were significantly different from others (MW,  $p < 0.05$ ).

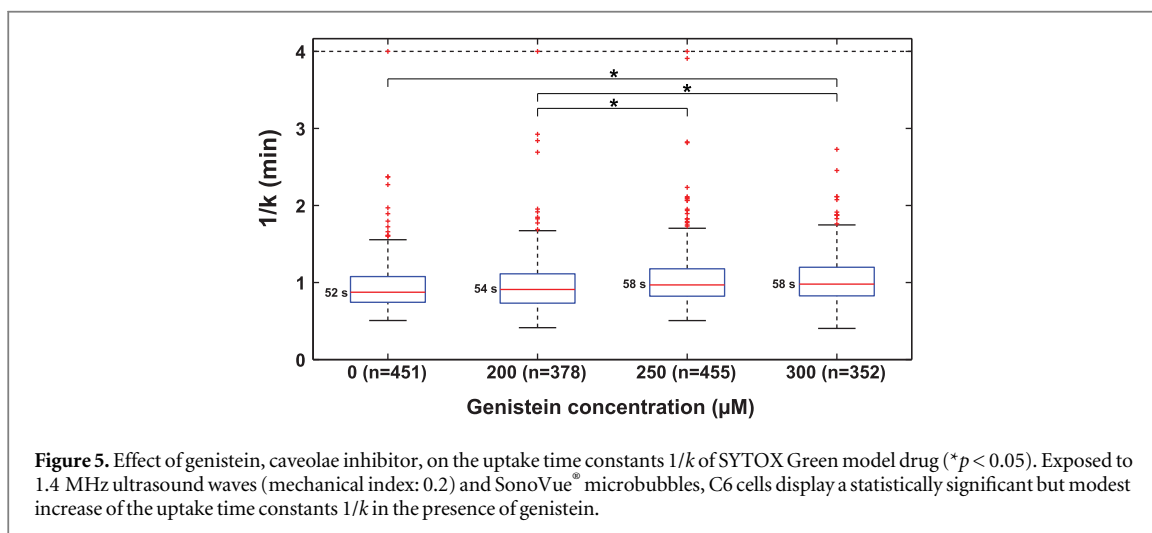
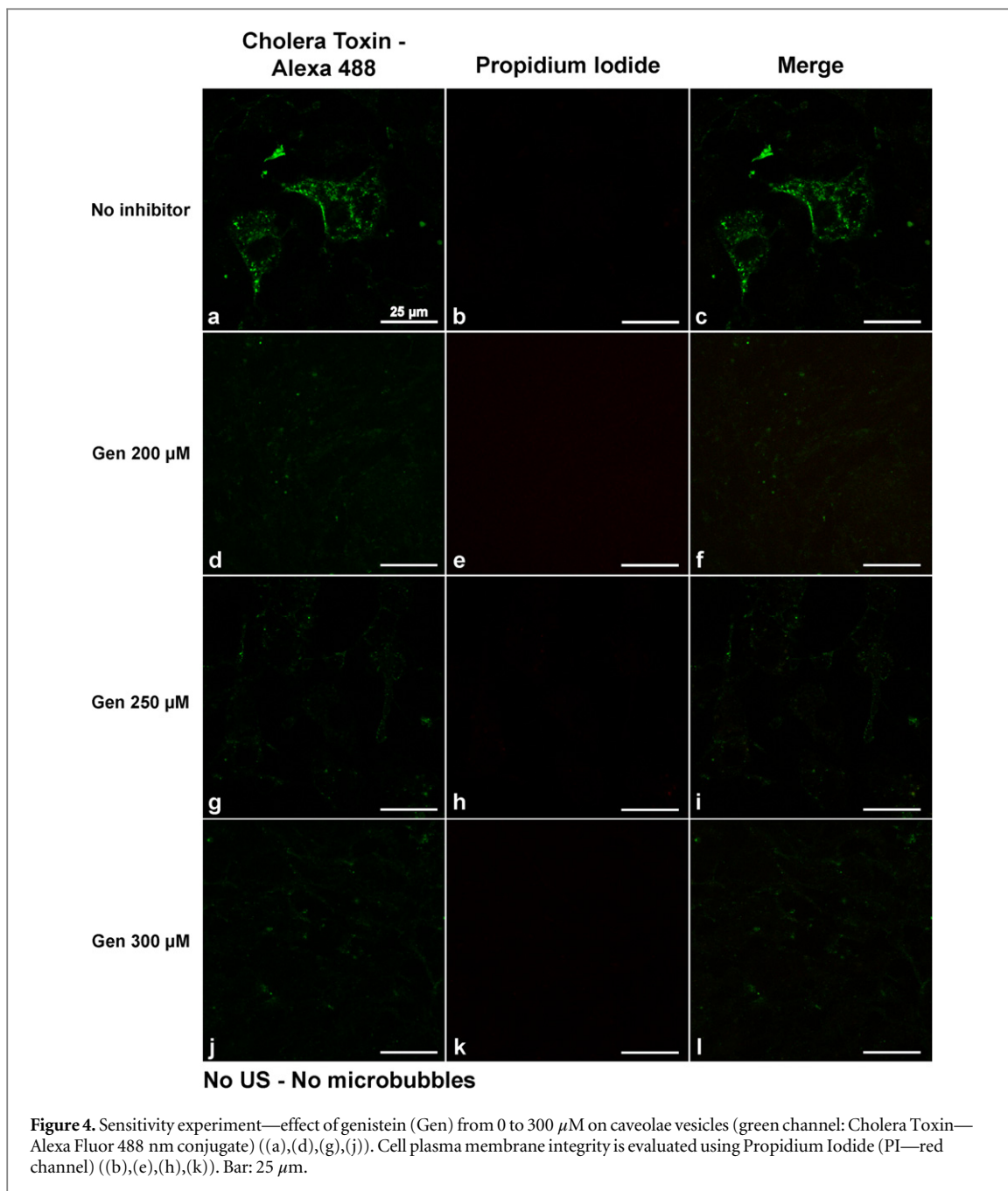
This dose-dependent response, where chlorpromazine led to slower intracellular transport of SYTOX Green, indicated hindrance of the clathrin-mediated pathway. As a corollary, these results imply the contribution of the clathrin-mediated pathway in the US-mediated uptake of SYTOX Green model drug. In addition, the increase of the time constants was larger for the inhibition of the clathrin-mediated pathway than for the inhibition of the caveolae-mediated pathway. Therefore, we infer that MB-assisted US primarily recruited the clathrin-mediated pathway.

An abrupt decrease of the time constant  $1/k$  was observed with chlorpromazine concentrations at 50 and 60  $\mu\text{M}$  (figure 6). The rapid sonopermeabilization-mediated uptake suggests a loss of cell membrane integrity, as also observed with the confocal images: 1 min 23 s (2 min 28 s,  $n = 448$ ) at 50  $\mu\text{M}$ , and 1 min 20 s (2 min 21 s,  $n = 242$ ), at 60  $\mu\text{M}$ . These time constants were not significantly different for these concentrations (MW,  $p = 0.54$ ).

## Discussion

A better understanding of sonopermeabilization bioeffects on tumor cell plasma membranes is required to potentially optimize delivery of poorly permeable anticancer agents. Here, we demonstrated the recruitment of endocytosis in sonopermeabilization-mediated delivery of small molecules (<4 kDa), *in vitro*, using real-time fluorescence imaging. In C6 rat glioma cells, we derived pharmacokinetic parameters derived from the fluorescence signal enhancement of a cell population [26]. This automated approach allowed us to quantify the effect of two endocytosis inhibitors, i.e. chlorpromazine and genistein, on the US-mediated uptake kinetics of SYTOX Green model drug.

The real-time monitoring of the model drug uptake showed a relation between the uptake time constants and the inhibitor concentration in a dose-dependent manner. With a significant 2.5-fold increase of the uptake time constant, chlorpromazine was found to have a higher effect on the slowing down of SYTOX Green uptake kinetics than genistein, whose time constant displayed a 1.1-fold increase. This suggests a predominant role of the clathrin-mediated pathway in sonopermeabilization-mediated drug delivery. These data raise the question of the key factors determining the preferred route of cellular entry



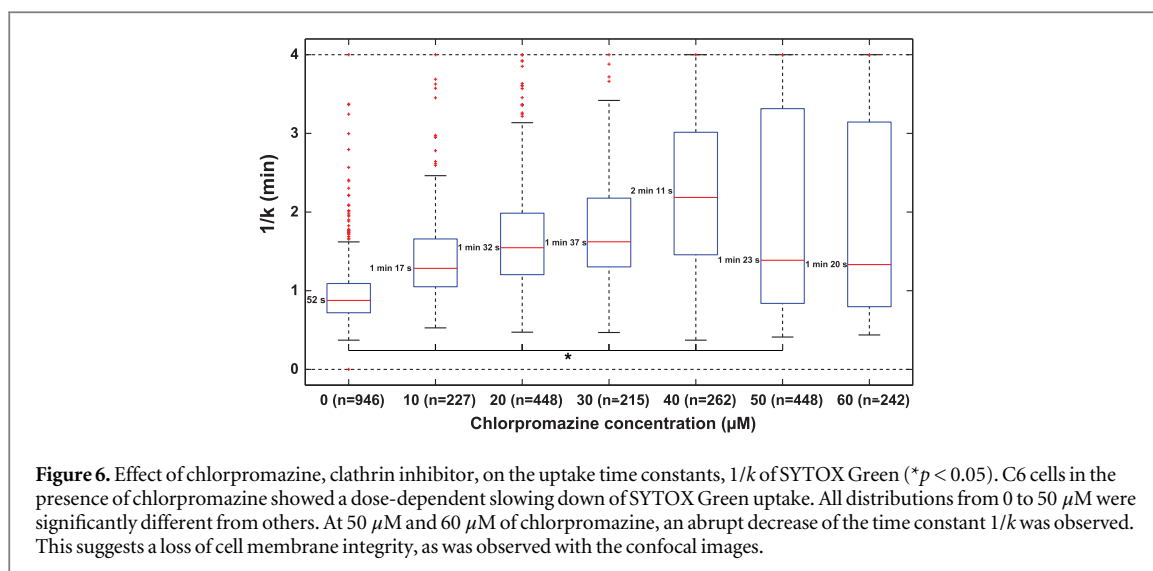


**Figure 6.** Effect of chlorpromazine, clathrin inhibitor, on the uptake time constants,  $1/k$  of SYTOX Green ( $*p < 0.05$ ). C6 cells in the presence of chlorpromazine showed a dose-dependent slowing down of SYTOX Green uptake. All distributions from 0 to 50  $\mu\text{M}$  were significantly different from others. At 50  $\mu\text{M}$  and 60  $\mu\text{M}$  of chlorpromazine, an abrupt decrease of the time constant  $1/k$  was observed. This suggests a loss of cell membrane integrity, as was observed with the confocal images.

when cells are sonopermeabilized. Meijering *et al* [18] showed that inhibition of clathrin-mediated endocytosis has a substantial effect on the cellular uptake of dextran macromolecules at different molecular weights (4.4–500 kDa), whereas the inhibition of caveolae-mediated endocytosis only affects internalization of larger molecules (155 and 500 kDa). Using a 600 Da model drug that is also found to be preferably taken up via the clathrin-mediated pathway, these findings would support the link between the molecular weight of the compound and its route of cellular entry. Conversely, using scanning electron microscopy, Zeghimi *et al* [21] showed primarily the recruitment of the caveolae-mediated pathway when U-87 MG human glioblastoma cells were exposed to US waves in presence of BR14<sup>®</sup> MBs. These results indicate that there might be other factors than the molecular weight influencing the route of cellular entry during sonopermeabilization, like the cell line, the US parameters and the type of MBs. Here, we quantified the recruitment of endocytosis with C6 cells only and limited our experiments to US exposures using 1.4 MHz and 0.2 MPa peak negative acoustic pressure, frequently used settings in sonopermeabilization studies. However, in US- and MB-mediated sonopermeabilization, acoustic pressure and frequency may have an impact on the nature of the internalization mechanism. These parameters may help optimize US- and MB-enhanced drug delivery, and should be considered in further investigations.

As shown by Vercauteren *et al* [33], the cytotoxicity of endocytosis inhibitors is cell line dependent, thus requiring a study of the viability of C6 cells preincubated with the endocytosis inhibitors. A cell viability higher than 50% could be found for chlorpromazine concentrations from 10 to 40  $\mu\text{M}$ , and concentrations from 200 to 250  $\mu\text{M}$  of genistein. Using laser scanning confocal microscopy, potential cytotoxicity of 50  $\mu\text{M}$  chlorpromazine was observed by the presence of PI fluorescence signal in the nuclei,

thus indicating the loss of plasma membrane integrity. Quantitative evaluation showed that the C6 cells preincubated with 50  $\mu\text{M}$  chlorpromazine displayed an abruptly accelerated uptake. Previous studies have shown that cells undergoing apoptosis might be permeable to small molecules, such as fluorescent dyes [41], providing a possible explanation of this rapid uptake due to the loss of plasma membrane integrity.

Our results provide a possible explanation for recent observations that cells may exhibit increased permeability for hours after sonopermeabilization [42]. In this scenario, pores are quickly resealed to maintain plasma membrane integrity, after which transport is continued by endocytosis recruitment.

The exact intracellular fate of the endocytic vesicles derived from US- and MB-induced cavitation is of interest. In this case, SYTOX Green is not free by diffusing in the cytoplasm, but is encapsulated in endocytic vesicles instead. However, it ultimately reaches the nucleus, and yields a fluorescence signal. Using high-resolution microscopy, further study investigating cell trafficking of these endocytic vesicles would help decipher these mechanisms.

## Conclusion

We have established *in vitro* the effect of two endocytosis inhibitors, i.e. chlorpromazine and genistein, on the pharmacokinetic parameters of a model drug uptake assessed in cell populations. Our approach showed that cells pretreated with endocytosis inhibitors and subsequently exposed to US in a presence of MB display slower uptakes, with a significant 2.5-fold increase of the uptake time constants with chlorpromazine concentration from 0 to 40  $\mu\text{M}$ , and a shallow but significant 1.1-fold increase of the uptake time constants with genistein from 0 to 300  $\mu\text{M}$ . These quantitative results support the recruitment of predominantly clathrin-mediated endocytosis in sonopermeabilization.

## Acknowledgments

This work was supported by Advanced ERC grant Sound Pharma—268906 (CM). The authors are grateful to Joep van den Dikkenberg and Georgi Nadibaidze for their technical support (Pharmaceutical Sciences Institute, University of Utrecht, Utrecht, the Netherlands). The data acquired with the Zeiss LSM 700 confocal microscope have been collected at the Cell Microscopy Core, Department of Cell Biology, University Medical Center Utrecht, Utrecht, Netherlands; the authors especially thank Corlinda ten Brink for her technical support.

## References

- [1] Sheikov N, McDannold N, Vykhodtseva N, Jolesz F and Hynynen K 2004 Cellular mechanisms of the blood-brain barrier opening induced by ultrasound in presence of microbubbles *Ultrasound Med. Biol.* **30** 979–89
- [2] Sheikov N et al 2006 Brain arterioles show more active vesicular transport of blood-borne tracer molecules than capillaries and venules after focused ultrasound-evoked opening of the blood–brain barrier *Ultrasound Med. Biol.* **32** 1399–409
- [3] Sheikov N, McDannold N, Sharma S and Hynynen K 2008 Effect of focused ultrasound applied with an ultrasound contrast agent on the tight junctional integrity of the brain microvascular endothelium *Ultrasound Med. Biol.* **34** 1093–104
- [4] Kotopoulis S, Dimceviski G, Gilja O H, Hoem D and Postema M 2013 Treatment of human pancreatic cancer using combined ultrasound, microbubbles, and gemcitabine: a clinical case study *Med. Phys.* **40** 072902
- [5] Escoffre J M, Novell A, Serrière S, Lecomte T and Bouakaz A 2013 Irinotecan delivery by microbubble-assisted ultrasound: *in vitro* validation and a pilot preclinical study *Mol. Pharm.* **10** 2667–75
- [6] Treat L H et al 2007 Targeted delivery of doxorubicin to the rat brain at therapeutic levels using MRI-guided focused ultrasound *Int. J. Cancer* **121** 901–7
- [7] Rapoport N Y, Kennedy A M, Shea J E, Scaife C L and Nam K H 2009 Controlled and targeted tumor chemotherapy by ultrasound-activated nanoemulsions/microbubbles *J. Control. Release* **138** 268–76
- [8] Park E J, Zhang Y Z, Vykhodtseva N and McDannold N 2012 Ultrasound-mediated blood–brain/blood–tumor barrier disruption improves outcomes with trastuzumab in a breast cancer brain metastasis model *J. Control. Release* **163** 277–84
- [9] Sasaki N et al 2012 Activation of microbubbles by short-pulsed ultrasound enhances the cytotoxic effect of cis-diamminedichloroplatinum (ii) in a canine thyroid adenocarcinoma cell line *in vitro Ultrasound Med. Biol.* **38** 109–18
- [10] Mehier-Humbert S, Bettinger T, Yan F and Guy R H 2005 Plasma membrane poration induced by ultrasound exposure: implication for drug delivery *J. Control. Release* **104** 213–22
- [11] Van Wamel A et al 2006 Vibrating microbubbles poking individual cells: drug transfer into cells via sonoporation *J. Control. Release* **112** 149–55
- [12] Schlicher R K et al 2006 Mechanism of intracellular delivery by acoustic cavitation *Ultrasound Med. Biol.* **32** 915–24
- [13] Miller D L, Pislaru S V and Greenleaf J F 2002 Sonoporation: mechanical DNA delivery by ultrasonic cavitation *Somat. Cell Mol. Genetics* **27** 115–34
- [14] Suslick K S 1988 *Ultrasound: its Chemical, Physical, and Biological Effects* (New York: VCH)
- [15] Zhou Y, Yang K, Cui J, Ye J Y and Deng C X 2012 Controlled permeation of cell membrane by single bubble acoustic cavitation *J. Control. Release* **157** 103–11
- [16] Kiyoshima D, Kawakami K, Hayakawa K, Tatsumi H and Sokabe M 2011 Force- and  $\text{Ca}^{2+}$ -dependent internalization of integrins in cultured endothelial cells *J. Cell. Sci.* **124** 1–12
- [17] Afadzi M et al 2013 Mechanisms of the ultrasound-mediated intracellular delivery of liposomes and dextrans *IEEE Trans. Ultrason. Ferroelectr. Freq. Control* **60** 21–33
- [18] Meijering B D M et al 2009 Ultrasound and microbubble-targeted delivery of macromolecules is regulated by induction of endocytosis and pore formation *Circ. Res.* **104** 679–87
- [19] Lee J L, Lo C W, Inserra C, Béra J C and Chen W S 2014 Ultrasound enhanced PEI-mediated gene delivery through increasing the intracellular calcium level and PKC- $\delta$  protein expression *Pharm. Res.* **31** 2354–66
- [20] Juffermans L J M, Meijering B D M, Henning R H and Deelman L E 2014 Ultrasound and microbubble-targeted delivery of small interfering RNA into primary endothelial cells is more effective than delivery of plasmid DNA *Ultrasound Med. Biol.* **40** 532–40
- [21] Zeghimi A, Escoffre J M and Bouakaz A 2013 Sonoporation, endocytosis and pore formation *19th European Symp. Ultrasound Contrast Imaging Rotterdam*
- [22] De Paula D M B, Valero-Lapchik V B, Paredes-Gamero E J and Han S W 2011 Therapeutic ultrasound promotes plasmid DNA uptake by clathrin-mediated endocytosis *J. Gene Med.* **13** 392–401
- [23] Lionetti V et al 2009 Enhanced caveolae-mediated endocytosis by diagnostic ultrasound *in vitro Ultrasound Med. Biol.* **35** 136–43
- [24] Fan Z, Liu H, Mayer M and Deng C X 2012 Spatiotemporally controlled single cell sonoporation *Proc. Natl Acad. Sci. USA* **109** 16486–91
- [25] Derieppe M et al 2013 Real-time assessment of ultrasound-mediated drug delivery using fibered confocal fluorescence microscopy *Mol. Imaging Biol.* **15** 3–11
- [26] Derieppe M, Denis de Senneville B, Kuijff H, Moonen C and Bos C 2014 Tracking of cell nuclei for assessment of *in vitro* uptake kinetics in ultrasound-mediated drug delivery using fibered confocal fluorescence microscopy *Mol. Imaging Biol.* **16** 642–51
- [27] Lepetit-Coiffé M et al 2013 Quantitative evaluation of ultrasound-mediated cellular uptake of a fluorescent model drug *Mol. Imaging Biol.* **15** 523–33
- [28] Wang J F, Wu C J, Zhang C M, Qiu Q Y and Zheng M 2009 Ultrasound-mediated microbubble destruction facilitates gene transfection in rat C6 glioma cells *Mol. Rep. Biol.* **36** 1263–7
- [29] Liu H L et al 2010 Blood–brain barrier disruption with focused ultrasound enhances delivery of chemotherapeutic drugs for glioblastoma treatment *Radiology* **255** 415–25
- [30] Burke C W, Klibanov A L, Sheehan J P and Price R J 2011 Inhibition of glioma growth by microbubble activation in a subcutaneous model using low duty cycle ultrasound without significant heating *J. Neurosurg.* **114** 1654–61
- [31] Ivanov A I 2008 Pharmacological inhibition of endocytic pathways: is it specific enough to be useful? In exocytosis and endocytosis *Methods in Molecular Biology* (New York: Humana) pp 15–33
- [32] Thors L, Alajakku K and Fowler C J 2007 The ‘specific’ tyrosine kinase inhibitor genistein inhibits the enzymic hydrolysis of anandamide: implications for anandamide uptake *Br. J. Pharmacol.* **150** 951–60
- [33] Vercauteren D et al 2010 The use of inhibitors to study endocytic pathways of gene carriers: optimization and pitfalls *Mol. Ther.* **18** 561–9
- [34] Roth B L, Poot M, Yue S T and Millard P J 1997 Bacterial viability and antibiotic susceptibility testing with SYTOX green nucleic acid stain *Appl. Environ. Microbiol.* **63** 2421–31 (<http://aem.asm.org/content/63/6/2421.short>)
- [35] Deckers R, Yudina A, Carδοit L C and Moonen C 2011 A fluorescent chromophore TOTO-3 as a ‘smart probe’ for the assessment of ultrasound-mediated local drug delivery *in vivo Contrast Media Mol. Imaging* **6** 267–74

- [36] Lammertink B, Deckers R, Storm G, Moonen C and Bos C 2015 Duration of ultrasound-mediated enhanced plasma membrane permeability *Int. J. Pharm.* **482** 92–8
- [37] Escoffre J M *et al* 2013 Microbubble attenuation and destruction: are they involved in sonoporation efficiency? *IEEE Trans. Ultrason. Ferroelectr. Freq. Control* **60** 46–52
- [38] Loy G and Zelinsky A 2003 Fast radial symmetry for detecting points of interest *IEEE Trans. Pattern Anal.* **25** 959–73
- [39] Horowitz S B 1972 The permeability of the amphibian oocyte nucleus *in situ* *J. Cell Biol.* **54** 609–25
- [40] Gerace L and Burke B 1988 Functional organization of the nuclear envelope *Ann. Rev. Cell Biol.* **4** 335–74
- [41] Oropesa-Ávila M *et al* 2013 Apoptotic microtubules delimit an active caspase free area in the cellular cortex during the execution phase of apoptosis *Cell Death Dis.* **4** e527
- [42] Yudina A, Lepetit-Coiffé M and Moonen C 2011 Evaluation of the temporal window for drug delivery following ultrasound-mediated membrane permeability enhancement *Mol. Imaging Biol.* **13** 239–49